



Research



Cite this article: Saldanha R, Ho Thanh MT, Krishnan N, Hehny H, Patteson A. 2024 Vimentin supports cell polarization by enhancing centrosome function and microtubule acetylation. *J. R. Soc. Interface* **21**: 20230641. <https://doi.org/10.1098/rsif.2023.0641>

Received: 2 November 2023

Accepted: 10 April 2024

Subject Category:

Life sciences—physics interface

Subject Areas:

biophysics, biomechanics

Keywords:

cytoskeleton, microtubules, vimentin, cell polarization, centrosome, wound healing

Author for correspondence:

Renita Saldanha

e-mail: rbsaldan@syr.edu

Electronic supplementary material is available online at <https://doi.org/10.6084/m9.figshare.c.7214490>.

Vimentin supports cell polarization by enhancing centrosome function and microtubule acetylation

Renita Saldanha^{1,2}, Minh Tri Ho Thanh^{1,2}, Nikhila Krishnan^{2,3}, Heidi Hehny^{2,3} and Alison Patteson^{1,2}

¹Physics Department, ²BioInspired Institute, and ³Department of Biology, Syracuse University, Syracuse, NY, USA

RS, 0009-0005-8914-5074; HH, 0000-0001-6660-5254

Cell polarity is important for controlling cell shape, motility and cell division processes. Vimentin intermediate filaments are important for cell migration and cell polarization in mesenchymal cells and assembly of vimentin and microtubule networks is dynamically coordinated, but the precise details of how vimentin mediates cell polarity remain unclear. Here, we characterize the effects of vimentin on the structure and function of the centrosome and the stability of microtubule filaments in wild-type and vimentin-null mouse embryonic fibroblasts. We find that vimentin mediates the structure of the pericentriolar material, promotes centrosome-mediated microtubule regrowth and increases the level of stable acetylated microtubules in the cell. Loss of vimentin also impairs centrosome repositioning during cell polarization and migration processes that occur during wound closure. Our results suggest that vimentin modulates centrosome structure and function as well as microtubule network stability, which has important implications for how cells establish proper cell polarization and persistent migration.

1. Introduction

Animal cells must be dynamic to move and change shape while also being stable and rigid to generate sustained polarized motion. Central to these features is the cell's cytoskeleton. The animal cell's cytoskeleton is comprised of three interconnected filamentous networks: F-actin, microtubules and intermediate filaments (IFs) [1]. These networks coordinate different functional aspects of the cell. Filamentous actin is the cell's main force-generating machinery, producing protrusive forces at the cell membrane and working with myosin motors to generate cellular contractile forces [2,3]. Microtubules are rigid polarized polymers that span the length of cell and direct cargo transport and organization within the cell [4–6], and IFs form a passive filamentous network that supports and stabilizes the cell [7–10]. Many cellular functions rely on coordinated cross-talk amongst these cytoskeletal networks, though there is much more known about how they work individually than together [11,12].

Vimentin is an IF protein that plays a pivotal role in sustaining the mechanical integrity and motility characteristics of mesenchymal cells. Its significance extends to various biological and pathological processes, notably in wound healing, where its absence in vimentin-null mice markedly impairs this function [13]. Furthermore, a strong association exists between vimentin expression and the enhanced metastasis and aggressive growth of tumours [14–16]. The mechanical behaviour of vimentin and other IF proteins is distinctively different from that of actin or tubulin networks. Vimentin networks are soft at low strain but stiffen and resist breakage when strongly

sheared or compressed [17,18]. This property significantly contributes to the viscoelasticity of cells [8,19,20], particularly under significant deformation, safeguarding cells from mechanical damage. Vimentin thus serves as a protective 'cushion', crucial for maintaining nuclear positioning and preventing nuclear damage during scenarios like three-dimensional migration or intense cellular confinement [7,20]. Beyond their mechanical roles, vimentin IFs profoundly influence a range of non-mechanical cellular functions [21,22]. They act as integral regulators of cellular signalling, providing a scaffold that interacts with and modulates various signalling proteins. Recent studies have linked IFs to the integration of signals related to the determination of cell size, cell proliferation, cell fate as well as cell adhesion and motility [23,24].

Several emerging studies point to a mutually reinforcing connection between vimentin IFs and the microtubule network [9,25–27]. Vimentin is an IF protein expressed in mesenchymal cells and highly invasive cancer cells [14,21,28]. Disruption of microtubules collapses the vimentin network [25] and likewise disrupting vimentin alters the microtubule network [27]. Vimentin has been shown to enhance the persistence of the microtubule network by serving as a stable long-standing template for new microtubule growth [9], and recent work has shown in reconstituted *in vitro* systems that vimentin stabilizes microtubules against depolymerization through direct interaction [26]. Together, these works highlight a subtle interplay between microtubules and vimentin that is important for polarized cell migration.

The cell's centrosome acts as the microtubule-organizing centre of the cell and serves as the main microtubule-nucleating organelle [29]. The centrosome is essential for whole-cell polarization and is typically positioned near the cell nucleus between the nucleus and the leading edge of the cell [30]. Vimentin IFs are also localized around the cell nucleus, forming a dense physical mesh in the perinuclear region of the cell [7,10,21,28]. Experiments with cells on patterned adhesive substrates show loss of vimentin increases variability in centrosome positioning [31]. Cells lacking vimentin also have impaired polarization [32–36], which suggests that vimentin might interact with both microtubules and their organizing centre, the centrosome.

Based on these studies, we hypothesized a functional link between vimentin and the cell's centrosome in establishing cell polarization and directed migration. Here, we report novel experimental data that addresses the role of vimentin IFs in centrosome structure and microtubule-nucleating function. Our results suggest new mechanisms by which vimentin mediates cell polarization and cross-talks with the cell's microtubule architecture.

2. Material and methods

2.1. Cell culture

Wild-type (*vim*^{+/+}), vimentin-null (*vim*^{-/-}) mouse embryonic fibroblasts (mEFs) were kindly provided by J. Ericsson (Abo Akademi University, Turku, Finland). Cells were maintained in Dulbecco's modified Eagle's medium including HEPES and sodium pyruvate supplemented with 10% fetal bovine serum, 1% penicillin–streptomycin and non-essential amino acids. Cell cultures were maintained at 37°C with 5% CO₂.

2.2. Immunofluorescence

Cells were fixed for immunofluorescence using methanol for 10 min at -20°C. Cell membranes were permeabilized with 0.05% Triton-X in phosphate-buffered saline (PBS) for 15 min at room temperature and blocked with 1% bovine serum albumin (BSA) for 1 h at room temperature. For vimentin visualization, cells were incubated with primary rabbit anti-vimentin antibody (Abcam) diluted 1:200 in 1% BSA in PBS for 1.5 h at room temperature; the secondary antibody anti-rabbit Alexa Fluor 555 (Invitrogen) was used at a dilution of 1:1000 in 1% BSA in PBS for 1 h at room temperature. For visualizing microtubules, we used primary alpha-tubulin rat antibody (Bio-rad) diluted 1:200 in 1% BSA in PBS for 1.5 h at room temperature and secondary antibody anti-rat Alexa Fluor 647 (Invitrogen) at a dilution of 1:1000 in 1% BSA in PBS for 1 h at room temperature. For visualizing acetylated microtubules, cells were incubated with primary acetylated tubulin mouse antibody (Sigma–Aldrich) diluted 1:200 in 1% BSA in PBS and incubated for 1.5 h at room temperature; secondary antibody anti-mouse Alexa Fluor 568 (Invitrogen) was used at a dilution of 1:1000 in 1% BSA in PBS for 1 h at room temperature. Cells were stained using Hoechst 33342 (Molecular Probes) for 1 h at room temperature. For visualizing centrosome, cells were incubated with primary Cdk5rap2 rabbit antibody (Bethyl Laboratories), gamma-tubulin rabbit antibody (Sigma–Aldrich), pericentrin rabbit antibody (Abcam), cenexin rabbit antibody (Protein tech) and centrin mouse antibody (EMD Millipore) diluted 1:1000 for centrin and 1:200 for other centrosomal proteins in 1% BSA in PBS for 1.5 h at room temperature; secondary antibody anti-mouse Alexa Fluor 488 (Invitrogen) for centrin and anti-rabbit Alexa Fluor 488 (Invitrogen) for other centrosomal proteins was used at a dilution of 1:1000 in 1% BSA in PBS for 1 h at room temperature. Cells were mounted using Prolong diamond antifade mountant (Life Technologies) for epifluorescence and confocal imaging.

2.3. Expansion microscopy

Cells were plated on 22 × 22 mm coverslips until they reached 90% confluence and fixed with ice-cold methanol at -20°C for 10 min followed by the immunofluorescence procedure mentioned above. The cells were stained with antibodies against vimentin and centrin. Expansion microscopy was performed using techniques similar to previously published protocols [37,38]. Briefly, the fixed cells were then incubated at 40°C overnight in incubation solution (30% acrylamide in 1× PBS). Next, 1 ml of freshly prepared gelation solution (20% acrylamide, 7% sodium acrylate, 0.04% bis-acrylamide, 0.5% APS and 0.5%

TEMED in 1× PBS) was added per coverslip and allowed to solidify on ice for 20 min, followed by incubation for 20 min at room temperature and additional 1.5 h at 30°C. The solidified gels were then sectioned into 4 mm gel punches using a disposable biopsy punch. The gel punches were then digested with digestion buffer overnight (0.5% Triton-X, 0.03% EDTA, 1 M Tris-HCl, pH 8, 11.7% sodium chloride and 1 U ml⁻¹ of proteinase K). Finally, the punches were subjected to a second round of immunofluorescence procedures with antibody concentration increased to twice of the initial concentration and allowed to expand in water overnight at 4°C. The expanded gel punches were then mounted on a 35 mm Mattek dish and imaged using Leica SP8 confocal microscope.

2.4. Western blot

Cell lysates were obtained by suspending the cells in lysis buffer (HSEG buffer pH 7.4–40 mM NaCl (Fischer Scientific), 5 mM EDTA (Fischer Scientific), 4% glycerol (Fischer Scientific), 20 mM NaF (Fischer Scientific), 1% TritonX-100 (Fischer Scientific), 1× protease inhibitor; 0.1 mM PMSF). Bio-Rad Protein Assay Kit II (Bio-Rad Laboratories) was used to measure the acetylated tubulin concentration from the post-nuclear supernatant collected from the lysates. Standard western blot procedures were performed. The nitrocellulose membranes were probed with primary acetylated tubulin mouse antibody (Sigma–Aldrich) and primary alpha-tubulin mouse (Sigma–Aldrich) antibody diluted in TBS-Tween20 (ThermoFischer) and incubated overnight at 4°C. The membranes were probed using mouse horseradish peroxidase-conjugated secondary antibody (Invitrogen) for 1 h at room temperature. The protein levels were visualized using Clarity™ western ECL (Bio-rad Laboratories) substrate and imaged using Bio-Rad ChemiDoc™ imager.

2.5. Microtubule re-nucleation experiments and microtubule analysis

Cells were first treated with 1 μM nocodazole (Sigma–Aldrich) for 30 min at room temperature to disrupt microtubule filaments. To allow for microtubule regrowth, nocodazole was washed out and cells were placed back in cell media. Cells were fixed at 0, 1, 2 and 5 min intervals after washout and stained for microtubules and vimentin. The microtubule regrowth was analysed by tracing the radial region of microtubules stemming from the cell centrosome. Tracing was done manually in FIJI-IMAGEJ software. A minimum of 75 cells were analysed over 3+ independent experiments per condition. For analysing microtubules after nocodazole treatment, we used the Source Steger's algorithm in curve trace [39] in FIJI-IMAGEJ and computed the total microtubule contour length per cell; a minimum of 90 cells were analysed over 3+ independent experiments per condition.

2.6. Scratch wound-healing assay

A monolayer of cells was created by culturing 5 × 10⁵ cells in a 35 mm glass bottom Petri dish overnight. Wounds were generated using a 10 μl pipette tip to scratch the monolayer. Following the scratch wound, cells were fixed at different time points (1, 2 and 4 h) post scratching. The monolayers were then stained for centrosome (cdk5rap2), microtubules (alpha-tubulin) and DNA (Hoechst 33342) and imaged using a Nikon epi-fluorescence microscope. Cells within 20 μm of the scratch were analysed for the centrosome position. Centrosome positioning with respect to the wound was analysed using FIJI-IMAGEJ. A minimum of 70 cells were analysed over 2+ independent experiments per condition.

2.7. Imaging

2.7.1. Epi-fluorescence imaging

Epi-fluorescence imaging was performed using a Nikon Eclipse Ti (Nikon Instruments) inverted microscope equipped with an Andor Technologies iXon em+ EMCCD camera (Andor Technologies). Cells were imaged using a Plan Fluor (NA of 1.49) 100× oil immersion objective.

2.7.2. Confocal imaging

Expansion microscopy images of centrosome and vimentin were obtained by using SP8 laser scanning confocal microscope with lightning equipped with HC PL APO 40×/1.10 W CORR CS2 0.65 water objective. Airyscan confocal imaging was used to image microtubules and acetylated microtubules. Images were obtained using Zeiss Airyscan LSM 980 confocal microscope equipped with Plan Apochromat 63× oil immersion objective with 1.4 NA, 8Y multiplex mode and GaAsP detector. Images obtained were processed using Airyscan processing technique from ZEISS ZEN 3.2 software. For the scratch assay, zoomed out images at 10× magnification were obtained using spinning disk confocal microscope (Yokogawa CSU-W1) on an inverted Nikon Ti-E microscope with Perfect focus imaged onto a Andor Zyla CMOS camera.

2.7.3. Statistics

Data are presented as a mean value ± s.e.m. The unpaired Student's *t*-test with 95% confidence level was used to determine statistical differences between distributions. Denotations: **p* ≤ 0.05; ***p* ≤ 0.01; ****p* ≤ 0.001; *****p* ≤ 0.0001; n.s., *p* > 0.05. *N*

represents number of independent experiments. n represents the number of cells. All the graphs and statistical analysis were done using GRAPHPAD PRISM version 9 (GraphPad Software, Inc.).

3. Results

3.1. Loss of vimentin perturbs the pericentriolar matrix

To investigate vimentin's role in cell polarization, we used laser scanning confocal and fluorescence microscopy to examine the centrosome in $\text{vim}^{+/+}$ mEFs and $\text{vim}^{-/-}$ mEFs (figure 1a). To label the centrosome, cells were fixed and stained for the centrosomal protein Cep215 (*cdk5rap2*), a major pericentriolar material (PCM) protein associated with the organization of microtubules from the centrosome [40,41]. Figure 1a shows immunofluorescence images of microtubules, Cep215 and vimentin taken by a confocal laser scanning microscope. In wild-type cells, as expected, there is a strong accumulation of tubulin at the centrosome with long microtubule filaments extending out radially. Interestingly, in $\text{vim}^{-/-}$ cells, there is less tubulin localized around the centrosome (figure 1b). Further, the centrosome itself (marked by Cep215) is noticeably more condensed and smaller in the $\text{vim}^{-/-}$ mEFs compared to $\text{vim}^{+/+}$ mEFs. In addition, we observe an accumulation of vimentin that colocalizes with the centrosome in wild-type cells (figure 1a).

Based on these observations, we next sought to quantify centrosome structure in $\text{vim}^{+/+}$ and $\text{vim}^{-/-}$ mEFs (figures 1 and 2). The centrosome is composed of two centrioles (a mother and daughter centriole) embedded in a dense matrix of PCM proteins (figure 1d, schematic). To examine the PCM and centriole structure, we fixed and labelled cells for multiple centrosomal proteins localized in either the PCM (Cep215, gamma-tubulin pericentrin) or centriole protein complexes (cenexin and centrin). We found that the loss of vimentin significantly decreased the mean projected area of the centrosome by 40% as marked by Cep215 (figure 1e, $p \leq 0.001$) and by 40% as marked by gamma-tubulin (figure 1f, $p \leq 0.001$), which indicates that loss of vimentin perturbs the pericentriolar matrix. There was no significant difference in centrosomal area observed by staining for pericentrin (figure 1g), but the intensity for cells lacking vimentin is lower compared to wild-type cells ($p < 0.001$, electronic supplementary material, figure S1c), suggesting cells lacking vimentin have less pericentrin protein localized to the centrosome.

Next, we considered the centriole proteins, cenexin and centrin. There was no significant difference in the mean area and intensity of these two centrosome proteins between wild-type and vimentin-null cells (figure 2a,b, electronic supplementary material, figure S1d,e). However, we did find an impact of vimentin on centriole positioning, namely the distance between centrioles was significantly greater in wild-type cells compared to vimentin-null cells (figure 2d). These measurements were obtained for cells with two centrioles. A small fraction of the cells had only one centriole or even less frequently three centrioles, though there was no statistically significant change in centriole number between the two cells (electronic supplementary material, figure S2b). From the data in figures 1 and 2, we conclude that loss of vimentin disrupts multiple PCM protein localization as well as centriole position but does not significantly affect the intracellular levels of centriole-associated proteins, cenexin and centrin.

To further examine vimentin and the centrosome structure, we used expansion microscopy to improve the resolution of the images (S2). The centrioles are approximately 200 nm in diameter, just within the spatial limit attainable by light microscopy (200–500 nm). Expansion microscopy overcomes this barrier by physically increasing the size of the specimen by embedding a specimen in a swellable polymer matrix. By swelling the samples, the physical distance between proteins in the cell increases, allowing smaller structures to be resolved by light microscopy.

Figure 3 shows representative expansion microscopy images of wild-type and vimentin-null cells labelled with antibodies against vimentin and centrin. In wild-type cells, two distinct centrioles are observable in the expansion microscopy images. An accumulation of vimentin is also observed in the proximity of the centrioles. In contrast, two distinct centrioles are not observable in most of the vimentin-null cells, suggesting the centrioles in vimentin-null cells are much closer together and not spatially resolved even after expansion microscopy. These results further indicate a role of vimentin in maintaining centrosome structure that could be related to supporting the PCM (figure 2) and maintaining the spatial distance between centrioles.

3.2. Loss of vimentin disrupts centrosome-mediated microtubule renucleation

Cep215, gamma-tubulin and pericentrin are PCM proteins associated with the organization and nucleation of microtubules from the centrosome [40–43]. Thus, based on our results from figure 1, we hypothesized that loss of vimentin may disrupt the microtubule nucleation function of the centrosome. To quantitatively analyse centrosome-mediated microtubule-nucleating activity, we performed nocodazole-washout microtubule renucleation assays in $\text{vim}^{+/+}$ and $\text{vim}^{-/-}$ mEFs (S2, figure 4a). Microtubules were first disassembled by treating cells with 1 μM nocodazole for 30 min, and then microtubule renucleation from the centrosome was examined at different times after nocodazole washout (0, 1, 2 and 5 min). Here, we note our choice to use nocodazole to disrupt the microtubule filaments compared to ice treatment, which is also commonly used. We found that ice was not as effective as the nocodazole conditions used here to remove the microtubule filaments. In particular, we found many cold-stable microtubules in the mEF, consistent with prior literature studies on the mEF cell type [44].

The rate of microtubule renucleation was quantified by tracing the area around the centrosome showing microtubules renucleation (figure 4b). At time = 0 min (post-nocodazole washout), the amount of tubulin at the centrosome is slightly lower in vimentin-null cells compared to wild-type cells (12% difference, $p = 0.04$). At 1 min of regrowth, the centrosome in $\text{vim}^{+/+}$ showed 28% more microtubule renucleation than in null-cells ($p < 0.001$), and by 2 min, regrowth was 33% greater in wild-type than null-cells ($p < 0.001$). At 5 min, renucleated microtubules span nearly the whole length of cell for both $\text{vim}^{+/+}$

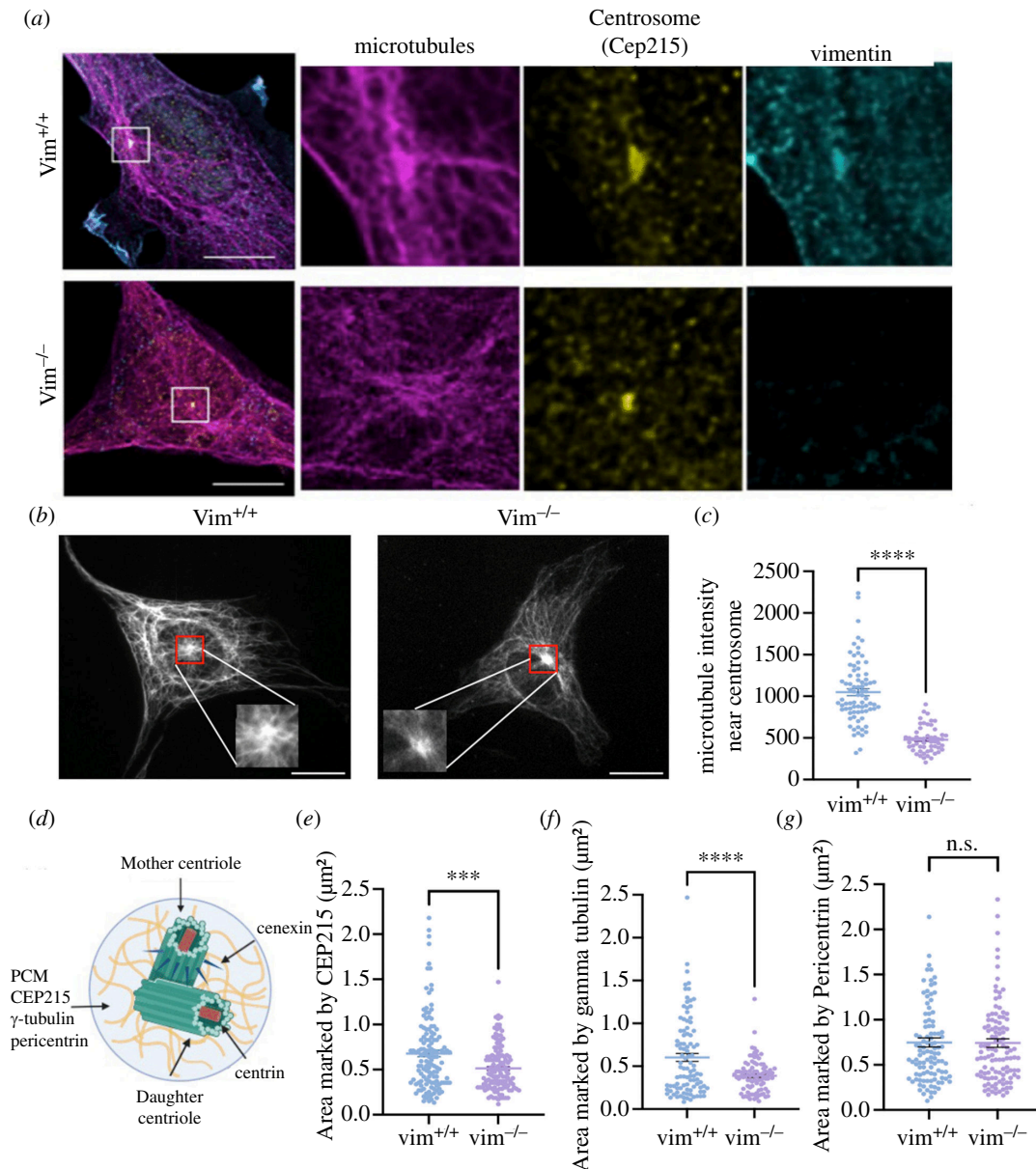


Figure 1. (a) Laser scanning confocal images of microtubules, centrosome (CEP215) and vimentin in $\text{vim}^{+/+}$ and $\text{vim}^{-/-}$ mEFs. (b) Epi-fluorescence microscopy images of microtubules originating from the centrosomes in $\text{vim}^{+/+}$ and $\text{vim}^{-/-}$ mEFs. The insets show zoomed-in images at the centrosome. (c) Quantification of microtubule intensity near the centrosome (marked as a red box in $\text{vim}^{-/-}$ cells) (d) Schematic of centrosome structure showing proteins associated with PCM and centrioles. (e–g) The projected area of the centrosome marked by CEP215, gamma-tubulin and pericentrin. Denotation: **** $p \leq 0.001$; ** $p \leq 0.01$ $n = 3$, $n > 90$ cells analysed per condition. Scale bar is $20 \mu\text{m}$.

and $\text{vim}^{-/-}$ mEFs (figure 4a). By computing the change in centrosome-nucleated microtubule area over 0–2 min, we find that the area of centrosome-nucleated microtubules grows at a rate 40% higher in $\text{vim}^{+/+}$ mEFs ($0.64 \mu\text{m}^2/\text{min}$) than $\text{vim}^{-/-}$ mEFs ($0.39 \mu\text{m}^2/\text{min}$) (figure 4c). While the nocodazole treatment does not completely annihilate the microtubules, the centrosome location is readily apparent, and we quantify microtubule regrowth only from the centrosome. Taken together, the results in figure 4 indicate vimentin may impact centrosome function by enhancing their microtubule-nucleation activity, which could contribute to vimentin's role in maintaining cell polarization.

3.3. Vimentin increases the amount of acetylated microtubules

On analysing the nocodazole-treated cells (figure 4), we observed the presence of stable microtubule filaments that remained in $\text{vim}^{+/+}$ mEFs but not $\text{vim}^{-/-}$ mEFs after sustained nocodazole treatment. As shown in figure 5a, after nocodazole treatment ($t=0$ min), a number of long microtubule filaments persist in wild-type mEF that are not observed in the null cells. To quantify the amount of remaining microtubules, microtubules were identified using a line/curve detection algorithm (Source Steger's algorithm, §2) and the total microtubule contour length was computed per cell. As shown in figure 5b, wild-type cells had a greater amount of nocodazole-resistant microtubule filaments than vimentin-null cells.

The presence of long-lived nocodazole-resistant microtubules in wild-type mEF indicates a change in microtubule dynamics and stability. This result is consistent with vimentin's role in supporting cell polarization and enhancing directed motion of

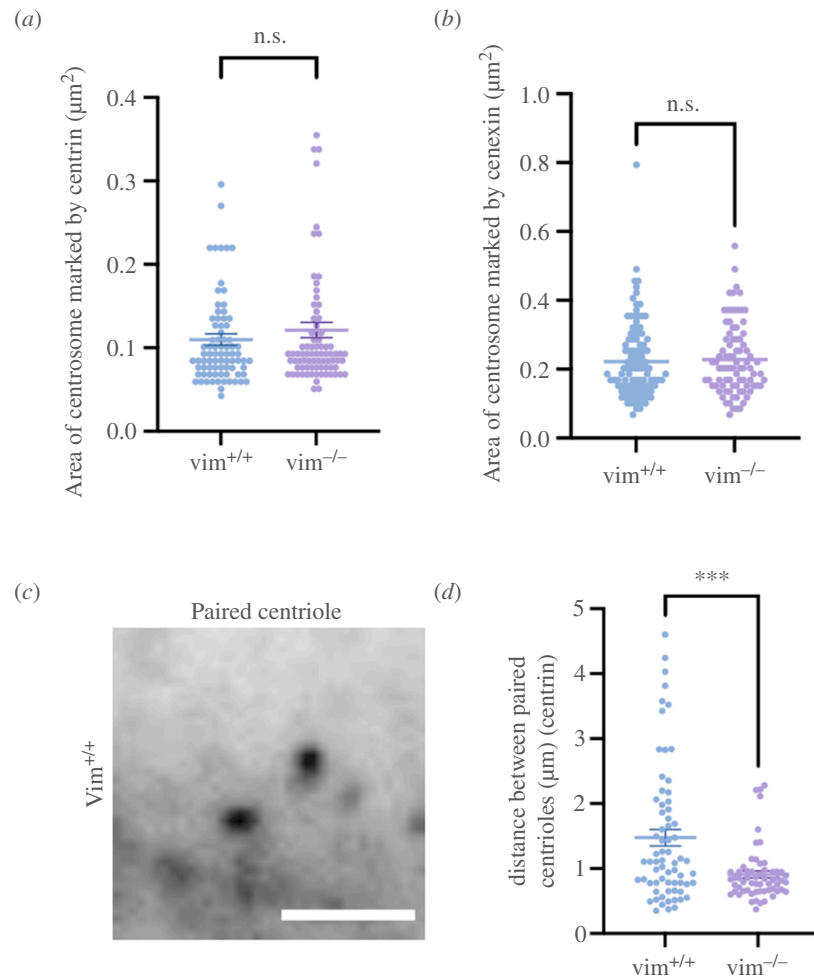


Figure 2. (a,b) The projected area of the centrosome marked by centriolar proteins centrin and cenexin. (c) Paired centrioles in $\text{vim}^{+/+}$ mEF cells. (d) Distance between the paired centrioles in $\text{vim}^{+/+}$ and $\text{vim}^{-/-}$ mEFs. Denotation: ***, $p \leq 0.001$; ns, $p > 0.05$ $n = 3$, $n > 90$ cells analysed per condition. Scale bar is 10 μm .

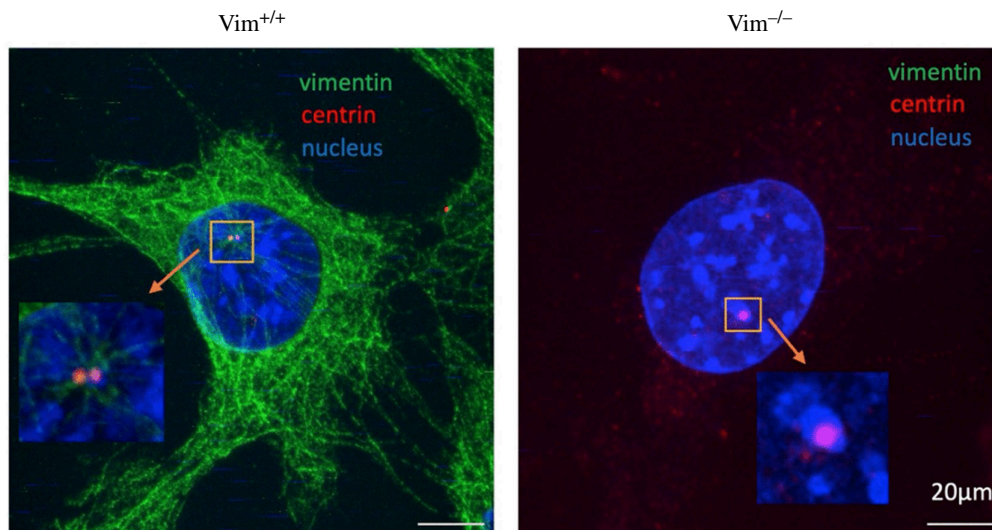


Figure 3. Expansion microscopy images for $\text{vim}^{+/+}$ and $\text{vim}^{-/-}$ cells stained for nucleus (blue), vimentin (green) and centrosome protein-centrin (red). The inset shows zoomed-in images at the centrosome.

cells [34]. Vimentin is known to fortify the microtubule network, serving as a template for new microtubule growth in a feedback mechanism that maintains cell polarity [9] and physically buttresses microtubule filaments against buckling and destabilization [45]. Microtubules dynamically assemble and disassemble with a turnover rate of 3–5 min [46]. Nocodazole disrupts microtubule networks by inhibiting microtubule polymerization; for nocodazole-treatment times greater than the microtubule turnover time, microtubules will depolymerize unless they have been stabilized, for instance by post-translational modifications. Acetylation is a post-translational modification in which an acetyl group is attached to the lysine group (K40) of alpha-tubulin [47]. Acetylation increases the flexibility of microtubules making them more resistant against mechanical forces

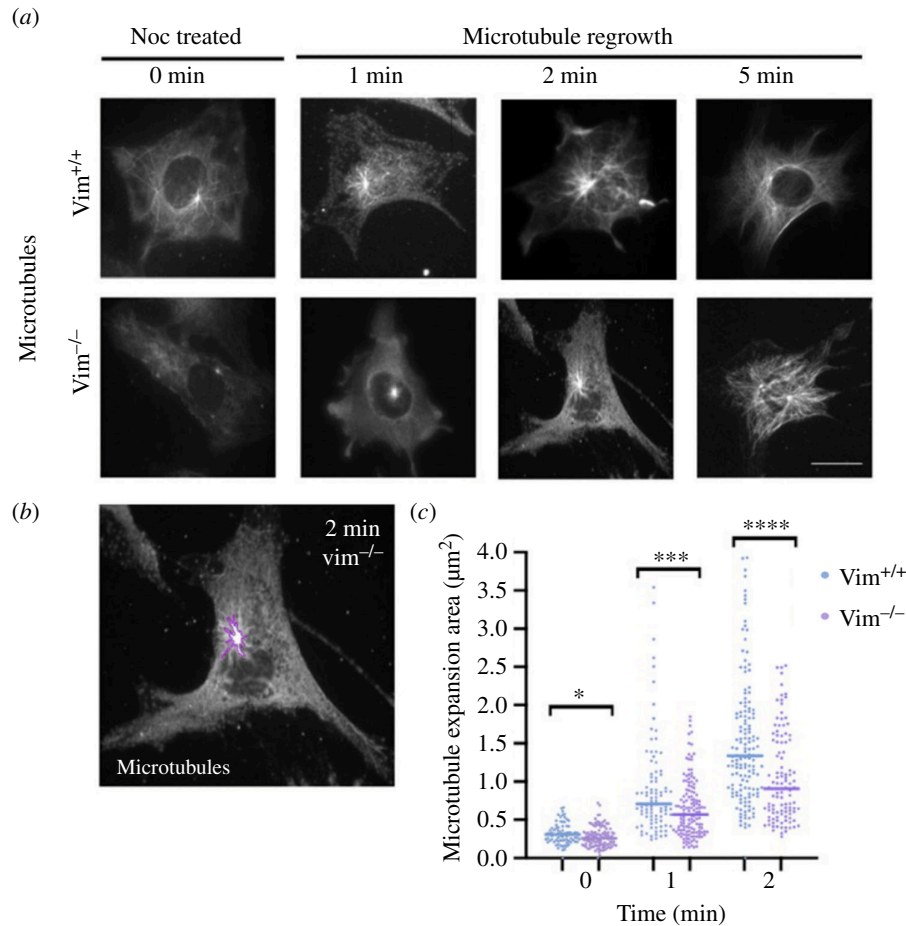


Figure 4. (a) Epi-fluorescence microscopy images of microtubules in *vim*^{+/+} and *vim*^{-/-} mEFs after nocodazole treatment (0 min) and regrowth at 1, 2 and 5 min after nocodazole washout. (b) The area marked to study microtubule renucleation. (c) The quantification of microtubule expansion area in *vim*^{+/+} and *vim*^{-/-} mEFs for 0, 1 and 2 min, respectively. Denotation: * $p \leq 0.05$; *** $p \leq 0.001$; n.s., $p > 0.05$. $n \geq 75$ cells analysed per condition, $n = 3$. The scale bar is 20 μm .

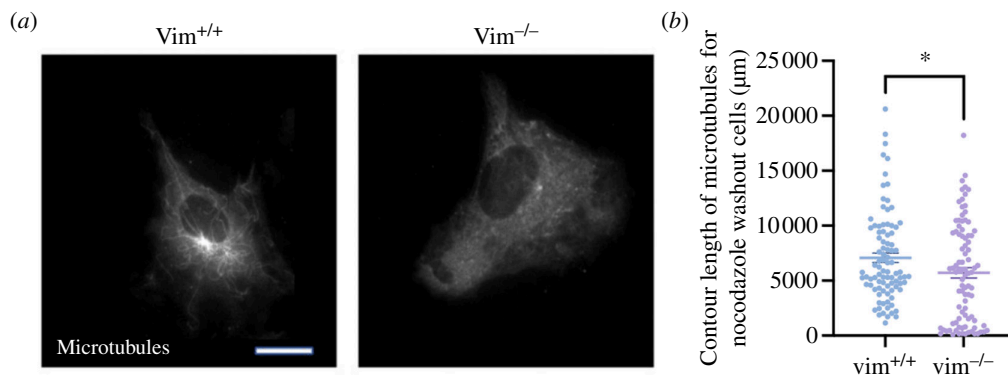


Figure 5. (a) Immunofluorescence images of microtubules in nocodazole-treated *vim*^{+/+} and *vim*^{-/-} mEFs. *Vim*^{+/+} mEFs show the presence of microtubules after 30 min of 1 μM nocodazole treatment (0 min after treatment). (b) Quantification of the contour length of the microtubules using the curve fit algorithm from FIJI-IMAGEJ. Denotation: * $p \leq 0.05$. $n > 90$ cells analysed per condition for $n = 3$. The scale bar is 20 μm .

and breakage [47]. In living cells, microtubules are frequently damaged and subsequently depolymerized; thus, acetylation protects against breaking and increases the stability of microtubules [48].

To investigate changes in microtubule acetylation levels, we next performed immunofluorescence and immunoblotting studies of acetylated tubulin, as shown in figure 6. Figure 6a shows immunofluorescence images of acetylated tubulin in *vim*^{+/+} and *vim*^{-/-} mEF. In wild-type cells, we observe significant amounts of acetylated tubulin that forms long filaments and a network-like structure in the cell. In contrast, in vimentin-null cells, the acetylated tubulin is much sparser and forms mostly small filamentous squiggles. We note that the mean spread area of vimentin-null cells is larger compared to wild-type cells (electronic supplementary material, figure S3). To further quantify the level of acetylated tubulin, we performed western blot experiments on the wild-type and vimentin-null cells. As shown in figure 6b, the mean immunofluorescence intensity of acetylated tubulin is approximately 20% higher in *vim*^{+/+} cells compared to *vim*^{-/-} cells ($p \leq 0.001$). The immunoblotting studies further confirmed that acetylated tubulin is higher in *vim*^{+/+} cells compared to *vim*^{-/-} cells whereas the total alpha-tubulin levels in both the cell lines are the same (figure 6c,d). Taken together, the results in figures 5 and 6 suggest vimentin positively influences the levels of microtubule acetylation, which enhances microtubule stability.

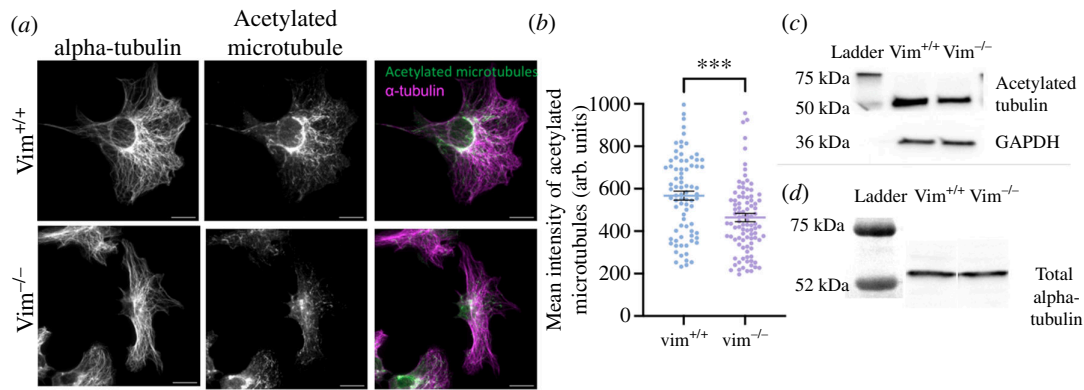


Figure 6. (a) Immunofluorescence images of acetylated microtubules for $\text{vim}^{+/+}$ and $\text{vim}^{-/-}$ mEFs. (b) Quantification of mean intensity of acetylated microtubules for $\text{vim}^{+/+}$ and $\text{vim}^{-/-}$ mEFs. Denotation: ***, $p \leq 0.001$. $n \geq 90$ cells analysed per condition, $n = 3$. (c) Western blot analysis for acetylated tubulin in $\text{vim}^{+/+}$ and $\text{vim}^{-/-}$ mEFs with GAPDH as control. (d) Western blot analysis for total alpha-tubulin in $\text{vim}^{+/+}$ and $\text{vim}^{-/-}$ cells. The scale bar is 20 μm .

3.4. Vimentin enhances repositioning of the centrosome towards the wound edge

Cells lacking vimentin have been shown to have decreased cell motility [32,49]. As the positioning of the centrosome is important for directional cell polarization and migration, we hypothesized vimentin would also impact the positioning of the centrosome in migrating cells. To study this, we performed an *in vitro* wound healing assay in $\text{vim}^{+/+}$ and $\text{vim}^{-/-}$ cells. The cells were fixed at 1, 2 and 4 h after making the scratch and stained for centrosomal protein Cep215, α -tubulin and the cell nucleus (DAPI) (figure 7a).

On two-dimensional surfaces, the cell centrosome is localized near the nucleus and its positioning between the cell nucleus and the leading edge of the cell tends to demark the polarized directionality of the cell. Upon wounding, fibroblasts at the edge of the wound become characteristically elongated and polarized with their long axis pointing in the direction of the open wound to facilitate wound healing. To investigate the role of vimentin in cell polarization upon wounding, we quantified the ability of the $\text{vim}^{+/+}$ and $\text{vim}^{-/-}$ mEF to reposition the cell centrosome toward the wound edge. Here, we estimated the cell polarization direction as the vector connecting the centre of the cell nucleus to the centrosome and measured its angular position with respect to the direction of the wound edge, with 180° indicating the centrosome was towards the wound and 0° away from the wound edge (figure 7b).

Figure 7d–f shows the probability distribution function (pdf) of centrosome angle for wild-type and vimentin-null fibroblasts near the wound edge (within 20 μm from scratch) at 1, 2 and 4 h post wounding (S2). As shown in figure 6d, at 1 h past wounding, both cell types exhibit a polarization toward the wound edge with a peak at approximately 150° , though there is no statistical difference between the two cell types. No significant differences in the centrosome positioning were observed for regions far away from the wound (electronic supplementary material, figure S4). At 2 h past wounding, the peak at 150° increases from a pdf value of 0.349–0.469 for wild-type cells but remains approximately the same for vimentin-null cells. At 4 h, a peak at 150° remains for wild-type cells, whereas the pdf is levelling out in vimentin-null cells. To further quantify the centrosome positioning, we calculated the percentage of cells with centrosome angles above and below a 120° threshold, with centrosome angle above 120° indicating a polarized direction toward the wound edge (table 1a). At 2 and 4 h post wounding, there is a statistically significant increase in polarized cells in wild-type mEF compared to vimentin-null mEF. At 2 h, approximately 65% of the $\text{vim}^{+/+}$ cells are polarized, whereas, for the $\text{vim}^{-/-}$ cells, only 40% of cells showed centrosomes aligned towards the wound ($p=0.0018$,**). At 4 h, again we see similar results, with 64% $\text{vim}^{+/+}$ cells having their centrosomes positioned towards the wound edge, compared to only 40% $\text{vim}^{-/-}$ cells ($p = 0.0007$,***). Taken together, the data in figure 7 indicate that vimentin enhances cell polarization during wounding healing and supports the repositioning of the centrosome towards the wound edge for directional cell migration to close the wound.

4. Discussion

Coordinated polarized cell migration requires an organized effort of three cytoskeletal networks, F-actin, microtubules and vimentin, but the details of how these distinct networks interact to enable cell motility remain largely unclear. Our results here suggest that vimentin networks are important for centrosome function and stabilize microtubule dynamics. In the presence of vimentin, we found that the size of centrosome is amplified, and centrosome-mediated microtubule nucleation is enhanced. The presence of vimentin also increases levels of microtubule acetylation, boosting microtubule stability in the cell. Further, during wound-healing experiments, vimentin increases repositioning of the cell centrosome toward the wound edge, supporting polarized cell migration to close the wound. From these observations, we propose that vimentin can modulate centrosome structure and function as well as microtubule network stability to enhance cell polarization.

One of the most pronounced phenotypes of vimentin-null mice is impaired wound healing [13,50]. *In vitro* wound-healing assays have shown that disrupting vimentin blocks directional migration and delays wound healing in several different cell types, including mEF [49], primary astrocytes [49], retinal pigment epithelial cells [9] and polyploid giant cancer cells [51]. This loss of directional wound healing can be attributed to a combination of factors, including reduced cell stiffness [19,20], altered nuclear positioning [10], altered cellular traction forces [33,36,52] and impaired directional migration [9,32]. Our results

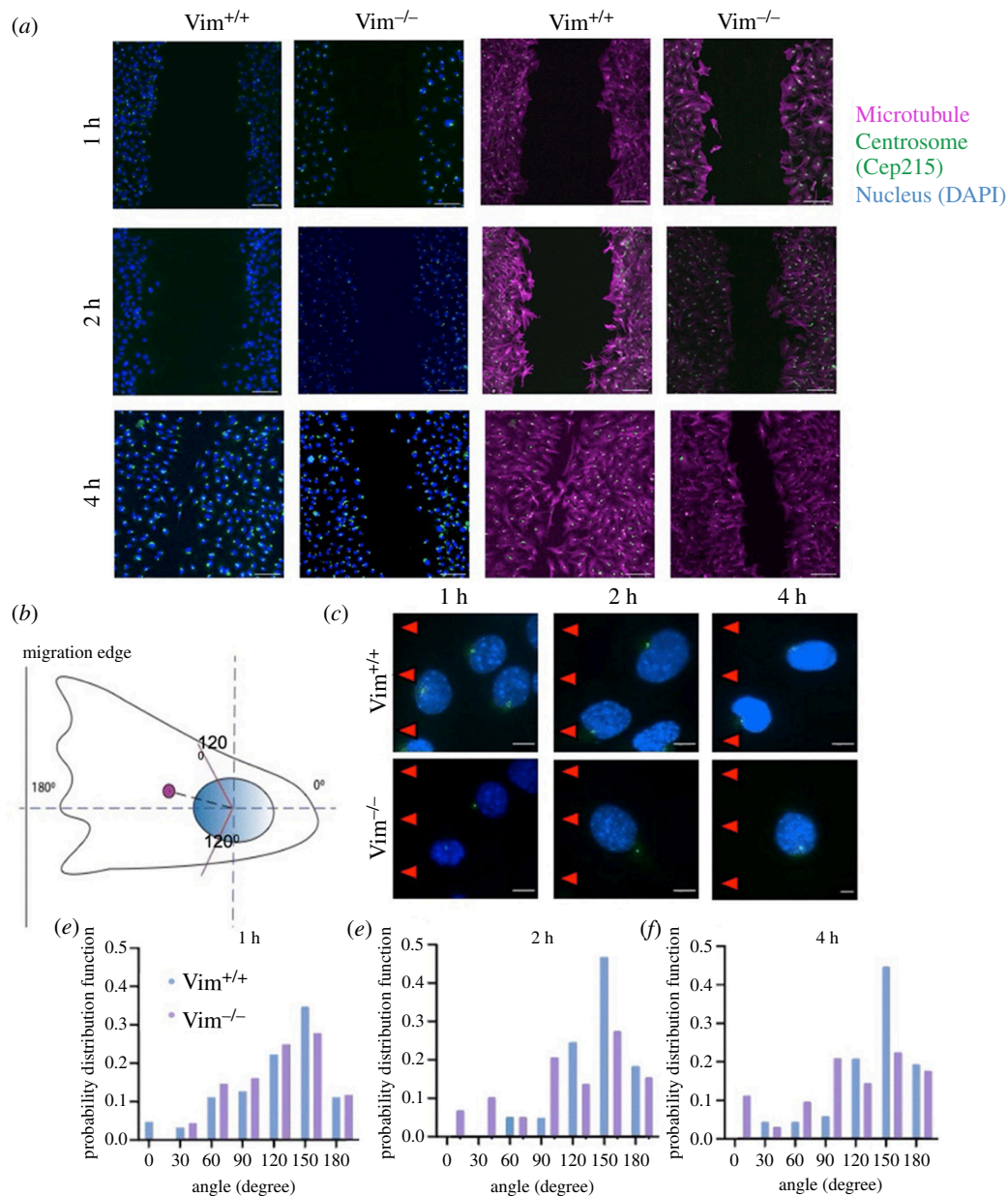


Figure 7. (a) Spinning disk confocal images of the nucleus (blue), centrosome protein Cep215 (green) and alpha-tubulin (magenta) for $vim^{+/+}$ and $vim^{-/-}$ mEFs fixed at 1, 2 and 4 h, respectively, after scratch using 10 \times objective. Scale bar is 100 μ m. (b) Schematic depicting of the angle made by the centrosome with respect to the centre of the nucleus as the origin axis, the red lines indicate 120 $^\circ$ angle (c) Zoomed-in images (100 \times objective) of centrosome (green) and nucleus (blue) of $vim^{+/+}$ and $vim^{-/-}$ cells near the wound edge (20 μ m from scratch) at 1, 2 and 4 h, respectively (with scratch to the left of the cell). The red arrows indicate the direction of wound. The scale bar is 10 μ m (d–f) quantification of the centrosome angle for $vim^{+/+}$ and $vim^{-/-}$ cells with respect to the nucleus at 1, 2 and 4 h, respectively. $n \geq 70$ cells analysed per condition, $n = 3$.

Table 1. Percentage of cells with centrosome angle above 120 $^\circ$. Percentage of $vim^{+/+}$ and $vim^{-/-}$ cells having centrosome angles above 120 $^\circ$ and p -values using chi-square test for 1, 2 and 4 h, respectively.

time (h)	$vim^{+/+}$	$vim^{-/-}$	p -value using chi-square test
1	54	60	0.3915, n.s.
2	65	43	0.0018**
4	64	40	0.0007***

shed new light on vimentin's role in wound healing via centrosome positioning and tubulin acetylation that are necessary for the proper polarization and directional motion for cells to heal wounds.

Recent work is revealing intricate, complex pathways at the signalling cross-roads among vimentin, microtubules and F-actin in coordinating cell dynamics. Prior work by Jiu *et al.* indicated that vimentin is antagonistic to actin stress fibre assembly through the microtubule-associated guanine nucleotide exchange factor GEF-H1 that activates RhoA [53]. FRAP studies showed loss of vimentin increased GEF-H1 dynamics and increased GEF-H1 phosphorylation on Ser886, which was attributed to

increased GEF-H1 activity in the absence of vimentin by using a phosphomimetic mutant protein [53]. Our results here suggest a possible parallel pathway for increased GEF-H1 activity in vimentin-deficient cells through altered microtubule acetylation (figure 5): we speculate that the increased levels of actin stress fibre assembly and cellular traction stresses in vimentin-deficient cells, which have been observed before, arises from the loss of stable acetylated microtubules, which releases GEF-H1 and increases the soluble pool of GEF-H1 that activates RhoA. On the other hand, recent work on microtubule acetylation by Seetharaman *et al.* would predict the reverse effect. Seetharaman *et al.* found that microtubule acetylation can promote the release of GEF-H1 from microtubules to activate RhoA and actomyosin contractility [54]. This indicates a mechanism by which GEF-H1 activity increases with the level of acetylated microtubules, which here is greater in wild-type than vimentin-null mEF and would thus predict an increase in actin stress fibre assembly and contractility in wild-type cells, which we note has been observed in some contexts, such as cells plated on soft substrates or in soft gels compared to on rigid substrates [45,49,55]. These two different expected effects of increased microtubule acetylation in vimentin-expressing cells on RhoA activity through GEF-H1 suggest at least two distinct biochemical signals that engage vimentin in regulating GEF-H1 activity and actin stress fibre formation. Of note, a recent study showed a link between centrosome amplification, an increased number of centrosomes commonly found in cancer cells, with increased tubulin acetylation levels [56]. Further, the polarized distribution of acetylated tubulin played a role in positioning the cell centrosome, distancing it away from the cell nucleus and organizing cell polarization.

Our results suggesting vimentin IFs impact centrosome size and function might be surprising, given that the primary function of the cell centrosome is organizing microtubules. Given the interdependent organization of vimentin and microtubules, early work in the IF field examined a possible link between vimentin and the centrosome [57,58]. Results have been mixed. One of the first studies using electron microscopy in 1985 found no direct interaction between centrioles and vimentin in HeLa cells [57], whereas later in 1995, an association between vimentin and PCM was found in SW-13 cells stably transfected with low levels of vimentin [58]. Our results indicate a possible functional role of vimentin in the microtubule-nucleating capacities of the centrosome. Our results suggest that vimentin impacts the size of the pericentriolar material of the cell centrosome, though it is not yet clear whether the change in size is due to altered spatial distribution of centrosomal protein or a change in the amount of PCM protein per centrosome, which are both possible structural changes for the centrosome [59]. While there are relatively few studies on the association of vimentin and the centrosome, we note that vimentin was identified in a 2003 proteomic characterization of the human centrosome by protein correlation profiling [60]. We note that one limitation of this study is that we did not measure intracellular levels of the pericentriolar proteins. Prior studies have indicated that the PCM behaves as a liquid condensate and the amount of pericentriolar material depends on the overall protein levels inside the cell [61,62]. It would be interesting in future studies to consider the effects of vimentin on transcriptional, translation or degradation levels of such proteins. Taken together, these works highlight a need to re-examine the link between vimentin, centrosome and its implications for whole cell organization and polarity.

Finally, our results here suggest new mechanisms by which vimentin coordinates polarized cell migration by regulating centrosome function and microtubule stability. Our recent work has shown loss of vimentin leads to abnormally persistent cell migration through confining microfluidic channels and that the presence of vimentin is needed for the ability of cells to stop and turn around [33,34]. In confining three-dimensional spaces, such as tissue, tight spaces add extra constraints and restrictions to motion of the cytoskeleton. In many (though not all) three-dimensional settings, the centrosome trails the cell nucleus, defining the tailing direction of the cell, and for the cell to change direction, the centrosome must reposition around the nucleus to a new trailing side of the cell [63]. We propose that by promoting centrosome activity vimentin boosts the ability of the centrosome to dynamically organize and reorganize microtubules and thus, the capacity of the cell to coordinate polarized, directional motion. The microtubule network stabilizing effect of vimentin may further allow the cell to build an internal compass that competes against externally imposed constraints.

5. Conclusion

Taken together, our results demonstrate a new role for VIFs in maintaining centrosome size and microtubule network stability. Our data provide evidence that VIFs are involved in regulating the microtubule-nucleating function of the cell centrosome and the expression levels of acetylated tubulin. Further, during wound-healing experiments, vimentin increases repositioning of the cell centrosome toward the wound edge, supporting polarized cell migration to close open wounds. Our results provide new insight into the coordinated cross-talk between vimentin and the microtubule networks in cell polarization.

Ethics. This work did not require ethical approval from a human subject or animal welfare committee.

Data accessibility. All data can be accessed from the Dryad digital repository [64].

Electronic supplementary material is available online [65].

Declaration of AI use. We have not used AI-assisted technologies in creating this article.

Authors' contributions. R.S.: conceptualization, data curation, formal analysis, investigation, methodology, visualization, writing—original draft; M.T.H.T.: conceptualization, investigation, visualization, writing—review and editing; H.H.: conceptualization, funding acquisition, resources, supervision, visualization, writing—review and editing; A.P.: conceptualization, funding acquisition, project administration, resources, supervision, validation, writing—review and editing; N.K.: investigation.

All authors gave final approval for publication and agreed to be held accountable for the work performed therein.

Conflict of interest declaration. We declare we have no competing interests.

Funding. This work was supported by NIH R35 GM142963 and NSF CMMI 2238600 awarded to A.P., an SU BioInspired Seed Grant awarded to H.H. and A.P., and by the National Institutes of Health grants R01GM127621 and R01GM130874 to H.H. Centrosome schematic was created with <https://www.biorender.com/>.

Acknowledgements. We thank J.M. Schwarz, Sarthak Gupta, Vladimir Gelfand, Paul Janmey and Annica Gad for useful and insightful discussions. We also thank Jennifer Ross for access and assistance with confocal imaging.

References

- Fletcher DA, Mullins RD. 2010 Cell mechanics and the cytoskeleton. *Nature* **463**, 485–492. (doi:10.1038/nature08908)
- Gardel ML, Schneider IC, Aratyn-Schaus Y, Waterman CM. 2010 Mechanical integration of actin and adhesion dynamics in cell migration. *Annu. Rev. Cell Dev. Biol.* **26**, 315–333. (doi:10.1146/annurev.cellbio.011209.122036)
- Murrell M, Oakes PW, Lenz M, Gardel ML. 2015 Forcing cells into shape: the mechanics of actomyosin contractility. *Nat. Rev. Mol. Cell Biol.* **16**, 486–498. (doi:10.1038/nrm4012)
- Kikumoto M, Kurachi M, Tosa V, Tashiro H. 2006 Flexural rigidity of individual microtubules measured by a buckling force with optical traps. *Biophys. J.* **90**, 1687–1696. (doi:10.1529/biophysj.104.055483)
- Meiring JCM, Shneyer BI, Akhmanova A. 2020 Generation and regulation of microtubule network asymmetry to drive cell polarity. *Curr. Opin. Cell Biol.* **62**, 86–95. (doi:10.1016/j.ccb.2019.10.004)
- Stehbens S, Wittmann T. 2012 Targeting and transport: how microtubules control focal adhesion dynamics. *J. Cell Biol.* **198**, 481–489. (doi:10.1083/jcb.201206050)
- Patteson AE *et al.* 2019 Vimentin protects cells against nuclear rupture and DNA damage during migration. *J. Cell Biol.* **218**, 4079–4092. (doi:10.1083/jcb.201902046)
- Guo M, Ehrlicher AJ, Mohammad S, Fabich H, Jensen MH, Moore JR, Fredberg JJ, Goldman RD, Weitz DA. 2013 The role of vimentin intermediate filaments in cortical and cytoplasmic mechanics. *Biophys. J.* **105**, 1562–1568. (doi:10.1016/j.bpj.2013.08.037)
- Gan Z *et al.* 2016 Vimentin intermediate filaments template microtubule networks to enhance persistence in cell polarity and directed migration. *Cell Syst.* **3**, 252–263. (doi:10.1016/j.cels.2016.08.007)
- Dupin I, Sakamoto Y, Etienne-Manneville S. 2011 Cytoplasmic intermediate filaments mediate actin-driven positioning of the nucleus. *J. Cell Sci.* **124**, 865–872. (doi:10.1242/jcs.076356)
- Huber F, Boire A, López MP, Koenderink GH. 2015 Cytoskeletal crosstalk: when three different personalities team up. *Curr. Opin. Cell Biol.* **32**, 39–47. (doi:10.1016/j.ccb.2014.10.005)
- Seetharaman S, Etienne-Manneville S. 2020 Cytoskeletal crosstalk in cell migration. *Trends Cell Biol.* **30**, 720–735. (doi:10.1016/j.tcb.2020.06.004)
- Eckes B, Colucci-Guyon E, Smola H, Nodder S, Babinet C, Krieg T, Martin P. 2000 Impaired wound healing in embryonic and adult mice lacking vimentin. *J. Cell Sci.* **113**, 2455–2462. (doi:10.1242/jcs.113.13.2455)
- Satelli A, Li S. 2011 Vimentin in cancer and its potential as a molecular target for cancer therapy. *Cell. Mol. Life Sci.* **68**, 3033–3046. (doi:10.1007/s00018-011-0735-1)
- Kidd ME, Shumaker DK, Ridge KM. 2014 The role of vimentin intermediate filaments in the progression of lung cancer. *Am. J. Respir. Cell Mol. Biol.* **50**, 1–6. (doi:10.1165/rcmb.2013-0314TR)
- Shi AM, Tao ZQ, Li R, Wang YQ, Wang X, Zhao J. 2016 Vimentin and post-translational modifications in cell motility during cancer - a review. *Eur. Rev. Med. Pharmacol. Sci.* **20**, 2603–2606.
- Qin Z, Kreplak L, Buehler MJ. 2009 Hierarchical structure controls nanomechanical properties of vimentin intermediate filaments. *PLoS One* **4**, e7294. (doi:10.1371/journal.pone.0007294)
- Janmey PA, Euteneuer U, Traub P, Schliwa M. 1991 Viscoelastic properties of vimentin compared with other filamentous biopolymer networks. *J. Cell Biol.* **113**, 155–160. (doi:10.1083/jcb.113.1.155)
- Mendez MG, Restle D, Janmey PA. 2014 Vimentin enhances cell elastic behavior and protects against compressive stress. *Biophys. J.* **107**, 314–323. (doi:10.1016/j.bpj.2014.04.050)
- Pogoda K *et al.* 2022 Unique role of vimentin networks in compression stiffening of cells and protection of nuclei from compressive stress. *Nano Lett.* **22**, 4725–4732. (doi:10.1021/acs.nanolett.2c00736)
- Patteson AE, Vahabikashi A, Goldman RD, Janmey PA. 2020 Mechanical and non-mechanical functions of filamentous and non-filamentous vimentin. *Bioessays* **42**, e2000078. (doi:10.1002/bies.202000078)
- Danielsson F, Peterson MK, Caldeira Araújo H, Lautenschläger F, Gad AKB. 2018 Vimentin diversity in health and disease. *Cells* **7**, 147. (doi:10.3390/cells7100147)
- Etienne-Manneville S. 2018 Cytoplasmic intermediate filaments in cell biology. *Annu. Rev. Cell Dev. Biol.* **34**, 1–28. (doi:10.1146/annurev-cellbio-100617-062534)
- Cheng F, Eriksson JE. 2017 Intermediate filaments and the regulation of cell motility during regeneration and wound healing. *Cold Spring Harb. Perspect. Biol.* **9**, a022046. (doi:10.1101/cshperspect.a022046)
- Yoon M, Moir RD, Prahlad V, Goldman RD. 1998 Motile properties of vimentin intermediate filament networks in living cells. *J. Cell Biol.* **143**, 147–157. (doi:10.1083/jcb.143.1.147)
- Schaedel L, Lorenz C, Schepers AV, Klumpp S, Köster S. 2021 Vimentin intermediate filaments stabilize dynamic microtubules by direct interactions. *Nat. Commun.* **12**, 3799. (doi:10.1038/s41467-021-23523-z)
- Goldman RD, Khuson S, Chou YH, Opal P, Steinert PM. 1996 The function of intermediate filaments in cell shape and cytoskeletal integrity. *J. Cell Biol.* **134**, 971–983. (doi:10.1083/jcb.134.4.971)
- Mendez MG, Kojima SI, Goldman RD. 2010 Vimentin induces changes in cell shape, motility, and adhesion during the epithelial to mesenchymal transition. *FASEB J.* **24**, 1838–1851. (doi:10.1096/fj.09-151639)
- Johnson A, Lewis J, Alberts B. 2002 *Molecular biology of the cell*. New York, NY: Garland Science.
- Luxton GWG, Gundersen GG. 2011 Orientation and function of the nuclear-centrosomal axis during cell migration. *Curr. Opin. Cell Biol.* **23**, 579–588. (doi:10.1016/j.ccb.2011.08.001)
- Shabbir SH, Cleland MM, Goldman RD, Mrksich M. 2014 Geometric control of vimentin intermediate filaments. *Biomaterials* **35**, 1359–1366. (doi:10.1016/j.biomaterials.2013.10.008)
- Helfand BT *et al.* 2011 Vimentin organization modulates the formation of lamellipodia. *Mol. Biol. Cell* **22**, 1274–1289. (doi:10.1091/mbc.E10-08-0699)
- Patteson AE *et al.* 2019 Loss of vimentin enhances cell motility through small confining spaces. *Small* **15**, e1903180. (doi:10.1002/sml.201903180)
- Gupta S, Patteson AE, Schwarz JM. 2021 The role of vimentin–nuclear interactions in persistent cell motility through confined spaces. *New J. Phys.* **23**, 093042. (doi:10.1088/1367-2630/ac2550)

35. Costigliola N, Ding L, Burckhardt CJ, Han SJ, Gutierrez E, Mota A, Groisman A, Mitchison TJ, Danuser G. 2017 Vimentin fibers orient traction stress. *Proc. Natl Acad. Sci. USA* **114**, 5195–5200. (doi:10.1073/pnas.1614610114)
36. Ho Thanh MT, Grella A, Kole D, Ambady S, Wen Q. 2021 Vimentin intermediate filaments modulate cell traction force but not cell sensitivity to substrate stiffness. *Cytoskeleton* **78**, 293–302. (doi:10.1002/cm.21675)
37. Krishnan N, Swoger M, Rathbun LI, Fioramonti PJ, Freshour J, Bates M, Patteson AE, Hehny H. 2022 Rab11 endosomes and pericentrin coordinate centrosome movement during pre-abscission *in vivo*. *Life Sci. Alliance* **5**, e202201362. (doi:10.26508/lsa.202201362)
38. Aljiboury A *et al.* 2022 Pericentriolar matrix (PCM) integrity relies on cenexin and polo-like kinase (PLK)1. *Mol. Biol. Cell* **33**, br14. (doi:10.1091/mbc.E22-01-0015)
39. Steger C. 2013 Unbiased extraction of lines with parabolic and Gaussian profiles. *Comput. Vis. Image Underst.* **117**, 97–112. (doi:10.1016/j.cviu.2012.08.007)
40. Graser S, Stierhof YD, Nigg EA. 2007 Cep68 and Cep215 (Cdk5rap2) are required for centrosome cohesion. *J. Cell Sci.* **120**, 4321–4331. (doi:10.1242/jcs.020248)
41. Fong KW, Choi YK, Rattner JB, Qi RZ. 2008 CDK5RAP2 is a pericentriolar protein that functions in centrosomal attachment of the gamma-tubulin ring complex. *Mol. Biol. Cell* **19**, 115–125. (doi:10.1091/mbc.e07-04-0371)
42. Dictenberg JB, Zimmermann W, Sparks CA, Young A, Vidair C, Zheng Y, Carrington W, Fay FS, Doxsey SJ. 1998 Pericentrin and gamma-tubulin form a protein complex and are organized into a novel lattice at the centrosome. *J. Cell Biol.* **141**, 163–174. (doi:10.1083/jcb.141.1.163)
43. Stearns T, Evans L, Kirschner M. 1991 Gamma-tubulin is a highly conserved component of the centrosome. *Cell* **65**, 825–836. (doi:10.1016/0092-8674(91)90390-k)
44. Bershadsky A, Gelfand V, Svitkina T, Tint I. 1979 Cold-stable microtubules in the cytoplasm of mouse embryo fibroblasts. *Cell Biol. Int. Rep.* **3**, 45–50. (doi:10.1016/0309-1651(79)90067-5)
45. Alisafaei F, Mandal K, Swoger M, Yang H, Guo M, Janmey PA, Patteson AE, Shenoy VB. 2022 Vimentin intermediate filaments can enhance or abate active cellular forces in a microenvironmental stiffness-dependent manner. *bioRxiv* 2022.04.02.486829. (doi:10.1101/2022.04.02.486829)
46. Shelden E, Wadsworth P. 1993 Observation and quantification of individual microtubule behavior *in vivo*: microtubule dynamics are cell-type specific. *J. Cell Biol.* **120**, 935–945. (doi:10.1083/jcb.120.4.935)
47. Janke C, Montagnac G. 2017 Causes and consequences of microtubule acetylation. *Curr. Biol.* **27**, R1287–R1292. (doi:10.1016/j.cub.2017.10.044)
48. Xu Z, Schaedel L, Portran D, Aguilar A, Gaillard J, Marinkovich MP, Théry M, Nachury MV. 2017 Microtubules acquire resistance from mechanical breakage through intraluminal acetylation. *Science* **356**, 328–332. (doi:10.1126/science.aai8764)
49. Eckes B *et al.* 1998 Impaired mechanical stability, migration and contractile capacity in vimentin-deficient fibroblasts. *J. Cell Sci.* **111**, 1897–1907. (doi:10.1242/jcs.111.13.1897)
50. Ridge KM, Eriksson JE, Pekny M, Goldman RD. 2022 Roles of vimentin in health and disease. *Genes Dev.* **36**, 391–407. (doi:10.1101/gad.349358.122)
51. Xuan B, Ghosh D, Jiang J, Shao R, Dawson MR. 2020 Vimentin filaments drive migratory persistence in polyploid cancer cells. *Proc. Natl Acad. Sci. USA* **117**, 26756–26765. (doi:10.1073/pnas.2011912117)
52. De Pascalis C *et al.* 2018 Intermediate filaments control collective migration by restricting traction forces and sustaining cell–cell contacts. *J. Cell Biol.* **217**, 3031–3044. (doi:10.1083/jcb.201801162)
53. Jiu Y, Peränen J, Schaible N, Cheng F, Eriksson JE, Krishnan R, Lappalainen P. 2017 Vimentin intermediate filaments control actin stress fiber assembly through GEF-H1 and RhoA. *J. Cell Sci.* **130**, 892–902. (doi:10.1242/jcs.196881)
54. Seetharaman S *et al.* 2022 Microtubules tune mechanosensitive cell responses. *Nat. Mater.* **21**, 366–377. (doi:10.1038/s41563-021-01108-x)
55. Vahabikashi A *et al.* 2019 Probe sensitivity to cortical versus intracellular cytoskeletal network stiffness. *Biophys. J.* **116**, 518–529. (doi:10.1016/j.bpj.2018.12.021)
56. Monteiro P, Yeon B, Wallis SS, Godinho SA. 2023 Centrosome amplification fine tunes tubulin acetylation to differentially control intracellular organization. *EMBO J.* **42**, e112812. (doi:10.15252/embj.2022112812)
57. Maro B, Paintrand M, Sauron ME, Paulin D, Bornens M. 1984 Vimentin filaments and centrosomes. Are they associated? *Exp. Cell Res.* **150**, 452–458. (doi:10.1016/0014-4827(84)90589-5)
58. Trevor KT, McGuiire JG, Leonova EV. 1995 Association of vimentin intermediate filaments with the centrosome. *J. Cell Sci.* **108**, 343–356. (doi:10.1242/jcs.108.1.343)
59. Sankaran DG, Stemm-Wolf AJ, McCurdy BL, Hariharan B, Pearson CG. 2020 A semi-automated machine learning-aided approach to quantitative analysis of centrosomes and microtubule organization. *J. Cell. Sci.* **133**, jcs243543. (doi:10.1242/jcs.243543)
60. Andersen JS, Wilkinson CJ, Mayor T, Mortensen P, Nigg EA, Mann M. 2003 Proteomic characterization of the human centrosome by protein correlation profiling. *Nature* **426**, 570–574. (doi:10.1038/nature02166)
61. Woodruff JB, Ferreira Gomes B, Widlund PO, Mahamid J, Honigsmann A, Hyman AA. 2017 The centrosome is a selective condensate that nucleates microtubules by concentrating tubulin. *Cell* **169**, 1066–1077. (doi:10.1016/j.cell.2017.05.028)
62. Jiang X, Ho DBT, Mahe K, Mia J, Sepulveda G, Antkowiak M, Jiang L, Yamada S, Jao LE. 2021 Condensation of pericentrin proteins in human cells illuminates phase separation in centrosome assembly. *J. Cell Sci.* **134**, jcs258897. (doi:10.1242/jcs.258897)
63. Zhang J, Wang Y li. 2017 Centrosome defines the rear of cells during mesenchymal migration. *Mol. Biol. Cell.* **28**, 3240–3251. (doi:10.1091/mbc.e17-06-0366)
64. Saldanha R, Krishnan N, Ho Thanh MT, Hehny H, Patteson A. 2024 Vimentin supports cell polarization by enhancing centrosome function and microtubule acetylation [Dataset]. Dryad (doi:10.5061/dryad.mcvdnc7d)
65. Saldanha R, Krishnan N, Thanh H, Tri M, Hehny H, Patteson AE. 2024 Supplementary material from: Vimentin supports cell polarization by enhancing centrosome function and microtubule acetylation. Figshare (doi:10.6084/m9.figshare.c.7214490)